Polyhedron 95 (2015) 75–80

Contents lists available at ScienceDirect

Polyhedron

journal homepage: www.elsevier.com/locate/poly

Intercalation of thiazole in layered solids. A 3D framework supported in dipolar and quadrupolar intermolecular interactions

F. Echevarría [a], A.A. Lemus-Santana [b], M. González [b], J. Rodríguez-Hernández [a,c], E. Reguera [b,*]

[a] Instituto de Ciencia y Tecnología de Materiales, La Habana, Cuba
[b] Centro de Investigación en Ciencia Aplicada y Tecnología Avanzada, Unidad Legaria, Instituto Politécnico Nacional, Mexico
[c] Instituto de Investigaciones en Materiales, UNAM, México, D.F., Mexico

ARTICLE INFO

Article history:
Received 3 February 2015
Accepted 14 April 2015
Available online 21 April 2015

Keywords:
Thiazole
Intercalation
Intermolecular interactions
Hybrid solids
Tetracyanonickelates

ABSTRACT

Thiazole molecule was intercalated between layers of $T[Ni(CN)_4]$ with T = Mn, Fe, Co, Ni. The formed hybrid inorganic–organic 3D solid crystallizes with an orthorhombic unit cell, in the *Pmna* space group, and it remains stable on heating up to 185 °C. From this temperature, the intercalated molecules evolve. Their crystal structure was solved and refined from powder X-ray diffraction data, complemented with structural information from IR and UV–Vis spectroscopies. Intercalates molecules were found coordinated through their N atom to the available axial positions of the metal T while the Ni atom preserves the planar coordination geometry. In the interlayer region, molecules coordinated to neighboring layers remain interacting through dipolar and quadrupolar interactions. In the resulting 3D solids, the layer adopt a rippled sheets configuration determined by the dipole–dipole intermolecular interactions. For Fe and Co a pronounced temperature dependent spin–orbit coupling was observed from the derived values for the effective magnetic moment. The magnetic behavior of this series of intercalated solids is determined by the co-existence of two types of interactions, between T metals centers within the layer, which has antiferromagnetic character, and the one observed for metals from neighboring layers through the π–π cloud overlapping between ring planes, which is ferromagnetic. For the solids obtained by intercalation of thiazole, the antiferromagnetic interaction dominates.

1. Introduction

Materials made from the assembling of inorganic and organic building units have received large attention in the last decades, mainly by the high diversity of construction blocks available and, in consequence, by the combinations of them, which result in practically infinite number of 1D, 2D and 3D structures [1,2]. With an appropriate election of building units, porous frameworks are formed which find applications for gas storage and separation [3], molecular sieving [4], catalysis [5], drug delivery [6], sensors [7], nanoreactors [8], and in biomedical assays [9]. The intercalation of organic molecules in layered inorganic solids is a convenient route to obtain hybrid porous materials with flexible framework sensible to external stimuli and with adjustable pore windows and pore volume [10]. Such hybrid porous solids have attractive properties for gas adsorption and separation [11], as molecular magnets [12] and show many other functionalities [13].

The intercalation of organic molecules in layered solids is an appropriate model to study the non-covalent interactions between neighboring molecules. The intercalated molecules remain confined to a small volume where they combine restrained configurations, highly defined orientations, with still some degrees of freedom, conditions otherwise difficult to achieve in bulk, and interact with a limited number of neighboring molecules. When the intercalated molecule is free to rotate, through thermal activation, for instance, the material provides a model for molecular nanomotors [14,15]. In the formed hybrid solid, two ways of electronic communications or interactions are available, within the layer and between neighboring layers through the intercalated molecules. When the layers contain paramagnetic ions, for example, their interaction within the layers and between layers could be of antiferromagnetic or ferromagnetic nature, depending of the involving ligands. In presence of π–π interactions between ligands linked to metal centers at the neighboring layers, the interaction is of ferromagnetic nature [12]. For some ligands and metals, thermal activated spin crossover behavior is observed [16]. An analogue effect can be induced by a pressure change [17] or by irradiating the sample with UV–Vis light [18]. Through the intercalation

* Corresponding author.
E-mail address: edilso.reguera@gmail.com (E. Reguera).

http://dx.doi.org/10.1016/j.poly.2015.04.016
0277-5387/

of organic molecules between inorganic layers, hybrid materials with a wide diversity of functionalities are obtained.

The tetracyanonickelate ion, $[Ni(CN)_4]^{2-}$, and its Pd and Pt analogues, form 2D solids of formula unit $T(H_2O)_2[M(CN)_4]\cdot xH_2O$ (M = Ni, Pd, Pt) when react with divalent transition metals (T). These kind of inorganic layers have shown conformational flexibility which responds to steric and electronic requirements from the molecules bonded to T metal. In this sense, tetracyanometallate layers behave differently to the common inorganic layers, which maintain a rigid lamellar configuration. Neighboring layers remains together through a network of hydrogen bonding interactions between the water molecules coordinated to the axial positions for the metal T with the weakly bonded ones located in the interlayer region [19]. These water molecules, both coordinated and weakly bonded, can be removed to intercalate organic molecules in the interlayers region. By this means it is possible to functionalize a hole gallery with specific organic functions. Tetracyanonickelate layers can be also regarded, as molecular building blocks, which induce transformations in the intercalated organic molecules to form a new 3D solid with unknown properties. When the intercalated molecule (L) remain coordinated to the T metal, 3D porous frameworks of formula unit $T(L)[Ni(CN)_4]$ are obtained. Different molecules are available to form such porous solids, among them, pyrazine and dipyridyl derivatives (4,4′-bipyridine, 4,4′-bipyridylacetylene, ...) [20]. The formed 3D porous frameworks have been evaluated for H_2 storage [21] and CO_2 sorption [20]. These molecules (pyrazine and dipyridyl derivatives) have two available pyridinic N atoms to form coordination bonds with the metal T on neighboring layers and by this reason, these molecules form pillars between layers, and porous frameworks of different pore size and geometry are obtained. The framework containing pyrazine as pillar and iron as T metal has been intensively studied because it shows spin crossover behavior activated by temperature, pressure and light [14,17,18]. When the intercalated molecule has only one pyridinic N atom, like imidazole and its derivatives, bimolecular pillars are formed by dipolar and quadrupolar interactions between neighboring molecules [12,22]. By this means it is possible to functionalize a hole gallery with specific organic functions. Tetracyanonickelate layers can be also regarded, as molecular building blocks, which induce transformations in the intercalated organic molecules to form a new 3D solid with unknown properties.

In this contribution, thiazole molecule is intercalated in layers of $T[Ni(CN)_4]$ (T = Mn, Fe, Co, Ni) in order to study the interaction between neighboring molecules and to characterize the 3D structure and related physical properties of the formed solids. Their structure was solved and refined from X-ray diffraction (XRD) powder data complemented with information from IR and UV–Vis spectroscopies and thermogravimetric curves. The interaction between thiazole molecules was studied from the refined crystal structure and low temperature magnetic measurements. To the best of our knowledge, no previous study has been reported for this series of thiazole intercalation compounds.

2. Experimental

The samples to be studied were prepared by the precipitation method, mixing diluted neutral aqueous solutions of $K_2[Ni(CN)_4]$, thiazole (Tzle) and of the involved divalent metals (T = Mn, Fe, Co, Ni), in appropriate molar ratio according to the expected formula unit for the solid to be formed, $T(Tzle)_2[Ni(CN)_4]$. The precipitated solid was washed several times with distilled water until to obtain a filtrate free of accompanying ions and then dried in air to constant weight. The nature of the solids as a metal tetracyanometallate and the presence of thiazole as intercalated species were established from IR and UV–Vis spectra. The thermogravimetric (TG) curves provided information on the materials thermal stability and on the absence of water in their composition. The formula unit was finally confirmed by chemical analyses from X-ray fluorescence data.

The IR and UV–Vis spectra were collected in the ATR and integration sphere modes, respectively, using Perking Elmer equipment. The TG curves were recorded in HR-mode under a nitrogen flow of 100 mL/min with a Q5000 thermobalance (from TA Instruments). XRD powder patterns were collected at room conditions in Bragg–Brentano geometry with Cu Kα1 radiation using a D8 Advance diffractometer (from Bruker). Crystal structures were solved using SHELXS program [23] from extracted intensities according to Le Bail method [24]. Physical considerations and information from the complementary techniques were used in order to select the appropriate structural model to be refined. Structure refinement was carried out with Rietveld method using FULLPROF program [25] and pseudo-Voigt peak shape function. The background was modeled by a third-order polynomial. The interatomic C–N and Ni–C distances were constrained to take values within certain limits considering previous structural studies on the $T[Ni(CN)_4]$ layers [19] and on analogous pillared solids [12,15,22].

The magnetic data, particularly, temperature dependence of the susceptibility and the magnetization versus applied magnetic field, were recorded in the 2–300 K temperature and from −4 T to 4 T at 2 K ranges, respectively, using a MPMS3 SQUID magnetometer (from Quantum Design). The calculated effective magnetic moment values (μ_{eff}) were corrected for the diamagnetic contribution. The susceptibility versus temperature curves were fitted using ANISOFIT program [26] to estimate the ZFS parameters (D and E). The dipole and quadrupole moments for the thiazole molecule were calculated using GAUSSIAN 09 software with DFT method, B3PW91 functional and 6-311+g(d,p) base.

3. Results and discussion

3.1. Characterization of the solids under study

The precipitation method and the exfoliation of previously prepared $T(H_2O)_2[Ni(CN)_4]$ layers using an appropriate solvent (e.g., 1-methyl 2-pyrrolidone [27]) for the intercalation of the organic molecule, produce the same hybrid solid but it has a greater crystallinity for the first preparative route. From this fact, the four solids under study were obtained by the precipitation method.

IR spectra provided conclusive clue on the nature of the formed solid during the samples preparation. The coordination of the thiazole molecule to the axial positions of the metal T is revealed by comparison of the recorded spectra with those corresponding to thiazole and the layered solids, $T(H_2O)_2[Ni(CN)_4]\cdot xH_2O$. IR spectrum of the inorganic block is composed by the vibrations within the layer, ν (CN), δ (Ni–C–N) and ν (Ni–C), and of those from the water molecules, both coordinated and weakly bonded (xH_2O). In the IR spectra of the precipitated solids, the absorption bands, ν (OH) and δ (H–O–H), related to the presence of water molecules in the material, are absent (see Supplementary information). These last vibrations appear as narrow bands at 3600 and 1620 cm^{-1}, respectively, for the coordinated water molecules, and as a broad absorption band in the 3000–3500 cm^{-1} spectral region from ν (OH) stretching vibration of the weakly bonded ones. The coordination of the metal T to the CN ligand at its N end involve the CN 5σ orbital, which has certain antibonding character. From this fact, an increase or decrease in the electron density donated by the axial ligand to the metal is detected as a slight frequency shift, negative or positive, respectively, for the ν (CN) stretching vibration. For the thiazole intercalated solids, the shift,

relative to the respective layers, is −22, −19, −15, −9 cm^{-1} for Mn, Fe, Co, and Ni, respectively (see Supplementary information). The thiazole molecule has a complex vibrational spectrum by the presence of many bending and combinations bands in the ring vibrations. Nevertheless, the comparison of thiazole IR spectrum before and after the complex formation reveals changes of intensity and frequency of the absorption bands (see Supplementary information). Such changes were ascribed to the formation of a coordination bond through the more basic pyridinic N atom while the thiol S atom remains uncoordinated.

The recorded UV–Vis spectra complemented the information derived from IR spectroscopy. In the visible spectral region appears absorption bands that correspond to d–d transitions of the involved T metals (Fe, Co, Ni) in octahedral coordination (see Supplementary information). Mn(2+) with a half filled 3d orbitals, has no d–d transitions. The strong absorption bands observed below 400 nm correspond to metal–ligand electronic charge transitions within the tetracyanonickelate anion. Analogue spectral features are observed for the potassium salt, $K_2[Ni(CN)_4]$. The coordination bond formation at the N end of the square planar building block involves minor frequency shifts in the charge transfer bands related with the charge redistribution within the T–N≡C–Ni chain, through the π^*-back bonding effect at the C end. The effect of the thiazole molecule coordination to the metal T is probably contributing to the absorption bands configuration below 400 nm.

The information derived from IR spectra concerning the anhydrous character for the formed solids is confirmed by the TG data. The TG curves are free of weight loss below 180 °C where the material decomposes with evolution of thiazole molecules (see Supplementary information). The weight loss in the 180–300 °C range corresponds to the evolution of two thiazole molecules per formula unit. Regarding the boiling point of thiazole (116–118 °C), the intercalated thiazole molecule evolves at relatively higher temperature, which is an additional evidence on the coordination bond formation of thiazole molecule to the metal T. The thermal effects observed from 300 °C were ascribed to the evolution of the CN ligands by the inorganic block decomposition.

The above discussed IR, UV–Vis and TG data provide conclusive evidence on the nature of the material under study as intercalation compounds of formula unit $T(Tzle)_2[Ni(CN)_4]$ where the thiazole molecules are found coordinated to the metal T while the Ni atom coordinated to the C end of the CN ligands preserves its planar coordination. This supposes that the solid 3D framework is supported by intermolecular interactions between molecules coordinated to neighboring layers.

3.2. Crystal structure

The four thiazole intercalated solids crystallize with an orthorhombic unit cell in the *Pmna* space group, with cell parameters (in Å): Mn: $a = 7.521(2)$, $b = 6.923(2)$, $c = 14.340(3)$; Fe: $a = 7.442(2)$, $b = 6.848(2)$, $c = 14.227(3)$; Co: $a = 7.414(2)$, $b = 6.831(2)$, $c = 14.186(3)$; Ni: $a = 7.373(2)$, $b = 6.783(2)$, $c = 14.145(3)$. Within the unit cell volume two formula units, $T(Tzle)_2[Ni(CN)_4]$, are accommodated ($Z = 2$). The initial atomic positions to be refined, within the *Pmna* space group, were proposed from the refined crystal structure for the imidazole analogue [12]. The S atom was located with the heavy metal method. The initial position for the C and N atoms in the thiazole ring were found using Fourier difference mapping calculated with he program SHELXS [23]. The derived structural model was then refined with the Rietveld method [25]. Details on the XRD data collection and processing are available from Supplementary information file. Fig. 1 shows the experimental XRD pattern, its fitting according to the refined structural model, and their difference for $Fe(Tzle)_2[Ni(CN)_4]$. Analogue pattern fitting were obtained for

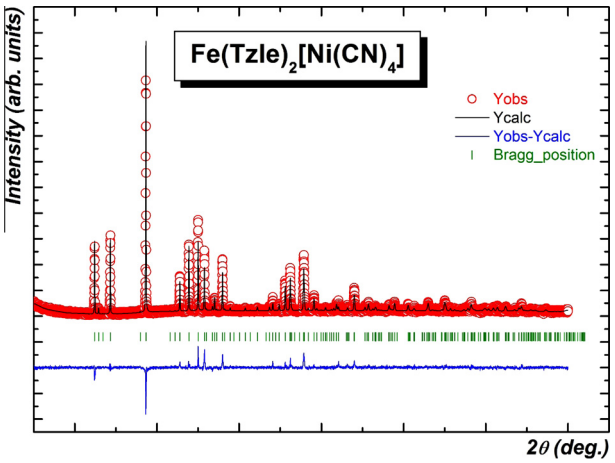

Fig. 1. XRD patterns, experimental, fitted and their difference, for $Fe(Tzle)_2[Ni(CN)_4]$. Analogue results from the structural refinement were obtained for Mn, Co, and Ni (see Supplementary information).

T = Mn, Co, Ni (see Supplementary information). In Fig. 2 the atomic packing within the unit cell is illustrated. As expected, according to the spectroscopic data, thiazole molecule occupies the axial positions for the metal T; and the Ni atom preserves its planar coordination to CN ligands. The information concerning to refined atomic positions and the calculated interatomic distance and angles is deposited in Cambridge Crystallographic Data Centre with the CCDC file numbers indicated below; it is also available from Supplementary information. According to the refined structure, the metal T is found with a distorted octahedral coordination; with certain axial elongation (Table 1). The energy splitting involved in this distortion remains below kT at room temperature (discussed below). The layers adopt an undulated or rippled sheets configuration determined by the intermolecular interactions in the interlayers region. For pillars formed by single molecules, like pyrazine and 4,4′-bipyridine , the layers are found with a planar configuration [20,21]. Thiazole is a molecule with dipole and quadrupole moments: $\mathbf{p} = 1.657$ D, and $\mathbf{Q}_{xx} = -31.0864$,

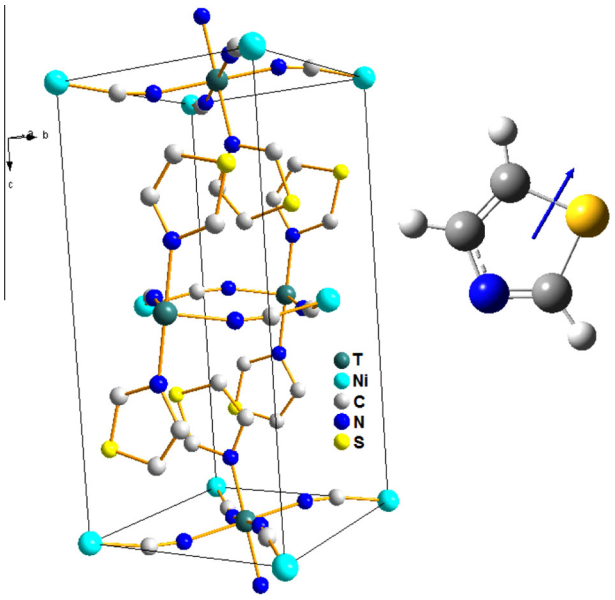

Fig. 2. Atomic packing and coordination environments for the atoms in the intercalated solids, $T(Tzle)_2[Ni(CN)_4]$ with T = Mn, Fe, Co, Ni. Thiazole molecule and its dipole moment (right side figure).

Table 1
Polarizing power* of the metal (T) and relevant structural information for the solids.

Metal (T)	Polarizing power, Ze/r^2	Cell volume (Å)	T–N_{Tzle} (Å)	T–N_{CN} (Å)	(T–T)$_{Tzle}$ (Å)	Ring–ring (Å)
Mn^{2+}	3.287	746.72 (2)	2.135 (1)	2.134 (2)	8.097 (1)	3.761 (2)
Fe^{2+}	3.463	725.05 (2)	2.117 (1)	2.085 (2)	8.028 (1)	3.721 (2)
Co^{2+}	3.652	718.45 (2)	2.111 (1)	2.068 (2)	8.004 (1)	3.707 (2)
Ni^{2+}	3.858	707.44 (2)	2.104 (1)	2.036 (2)	7.976 (1)	3.687 (2)

* The values for the metal polarizing power were taken from Ref. [29].

$\mathbf{Q}_{yy} = -31.7523$, $\mathbf{Q}_{zz} = -38.7752$ in D.Å, respectively. In the interlayer region, neighboring thiazole molecules are interacting through their dipole and quadrupole moments. The dipole moment of neighboring molecules are disposed with an antiparallel orientation, which is an attractive coupling (Fig. 2). Neighboring molecules are found in sandwich configuration or coplanar stacking (∠ ring–ring = 180°). Thiazole molecule has a relatively large negative quadrupole moment, which is not favorable for a sandwich configuration between neighboring molecules. For instance, for benzene, with a large negative quadrupole moment, the T shaped configuration is the most stable one [28]. It seems, the cooperative dipolar interaction of thiazole molecules in the interlayer region is determining both, their coplanar stacking, and the observed rippled sheet configuration for the layers (Fig. 3).

Table 1 summarizes the relevant structural information for the material under study. The unit cell volume, the bond distance for the ring to the metal (T–N_{Tzle}), the distance between metal centers from neighboring layers (T–T)$_{Tzle}$, and the ring-ring distance follow a positive correlation with the inverse of the metal polarizing power (Ze/r^2). For the most polarizing metal (Ni), the smallest cell volume and the shortest T–N_{Tzle}, T–T and ring–ring distances are observed. The polarizing power senses the metal ability to subtract electronic charge from the ligand and, in consequence, to enhance the metal–ligand coordination bond. This explains the correlation observed in Table 1, and also the above discussed negative frequency shift for ν (CN) stretching vibration. The coordination bond formation modifies the electronic charge distribution on the molecule and its dipole and quadrupole moments, favoring the attractive interactions between neighboring molecules, which is sensed as a reduction in the ring-ring distance for the metal of higher polarizing power.

3.3. Spin–orbit coupling and zero field splitting

As already discussed, the metal T is found in a distorted octahedral coordination environment formed by the N end of four CN groups plus two N atoms from thiazole molecules occupying the axial positions. For Fe and Co in an octahedral environment, with four and five electrons in t_{2g} orbitals (d_{xy}, d_{xz}, d_{yz}), respectively, the spin–orbit coupling is possible, depending on the splitting of the energy of levels (ΔE) relative to the thermal energy (kT). For Mn and Ni, with half-filled and filled t_{2g} orbitals, respectively, the presence of spin–orbit coupling is also possible by mixing of ground and excited states [30]. The presence of spin–orbit is sensed by the value of the effective magnetic moment (μ_{eff}) in the paramagnetic region, which can be calculated from the recorded magnetic susceptibility (χ_M) curve, according to: $\mu_{eff} = 2.828\ \mathrm{sqrt}(\chi_M T)$ [31]. Table 2 summarizes the values found for μ_{eff}, at room temperature, for the four metals. As expected, for Fe and Co the calculated values for μ_{eff} suggest the presence of spin–orbit coupling. A conclusive evidence in that sense is obtained from the dependence of μ_{eff} versus temperature curve (Fig. 4). For Ni the value of μ_{eff} corresponds to the value expected in presence of spin–orbit coupling, which could ascribed to a contribution of excited states or to zero-field splitting effect (discussed below). The value found for Mn, remains within the expected range for only spin contribution to the magnetic moment. For these last two metals (Mn and Ni), within the paramagnetic temperature

Table 2
Magnetic susceptibility values (in Bohr magneton unit) at room temperature (300 K) for T(Tzle)$_2$[Ni(CN)$_4$].

Metal (T^{2+})	Experimental value	Expected value* (spin + orbital)	Expected value* (spin only)	Unpaired electrons
Mn^{2+}	5.83	5.9	5.92	$5e^-$
Fe^{2+}	6.33	5.1–5.5	4.9	$4e^-$
Co^{2+}	5.18	4.1–5.2	3.87	$3e^-$
Ni^{2+}	4.39	2.8–4.0	2.83	$2e^-$

* Taken from Ref. [31] for an octahedral coordination.

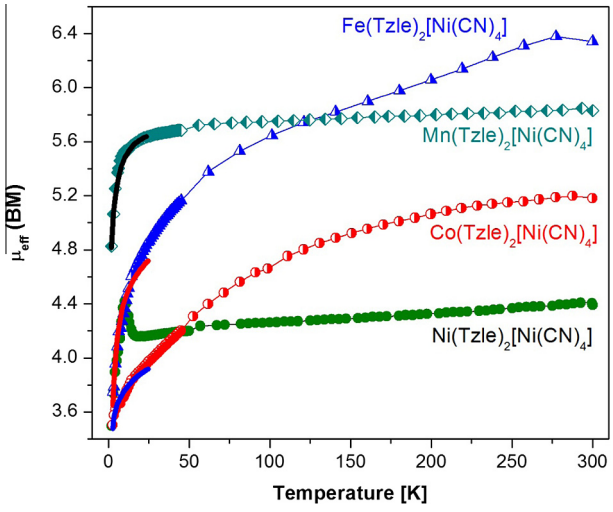

Fig. 3. Effective magnetic moment versus temperature for the series of thiazole intercalated solids, T(Tzle)$_2$[Ni(CN)$_4$] with T = Mn, Fe, Co, Ni. The region below 25 K was fitted using ANISOFIT program in order to estimate the ZFS parameters for Mn, Fe and Co.

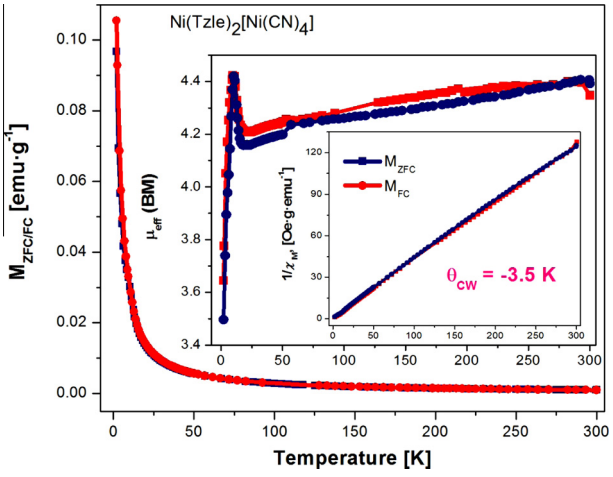

Fig. 4. Zero field cooling/field cooling magnetization curves for Ni(Tzle)$_2$[Ni(CN)$_4$]. Inset 1: effective magnetic moment versus temperature. Inset 2: inverse of susceptibility versus temperature curve indicating the presence of an antiferromagnetic interaction between Ni atoms.

region, the values of μ_{eff} remain without appreciable changes but, for Fe and Co, a progressive decrease for the value of this parameter is detected, to finally reach the value expected in the absence of orbital contribution. At high temperatures, the thermal energy (kT) is sufficient to compensate the energy splitting originated by the distortion from the octahedral environment. In this condition, all the electrons located in t_{2g} orbitals remain in degenerated states, which makes possible the occurrence of spin–orbit coupling. On cooling, the thermal energy (kT) decreases, and the orbital contribution to the magnetic moment progressively disappears. The thermal energy kT at room temperature (20 °C) is 0.04 eV. Then, the energy splitting in the t_{2g} orbitals, related with the coordination environment for the metal (T), remains below this value.

For Mn, Fe and Co, below 25 K, the effective magnetic moment (μ_{eff}) versus temperature curve shows a sudden decrease which, was ascribed to presence of zero-field splitting (ZFS) related to the spin microstates degeneration removal. The ZFS together with the spin–orbit coupling determine the anisotropy in the magnetic properties of coordination compounds containing transition metal ions [30]. At low temperature, the spin–orbit contribution is minimized, and the mentioned temperature dependence for the magnetic moment reveals the presence of ZFS effect. From this fact, in order to estimate the ZFS parameters (D and E), the low temperature region, below 25 K, of the μ_{eff} versus temperature curve was fitted using ANISOFIT program [26]. These fittings produce the following values, in cm^{-1}, for D and E: Mn: 4.4 and 0.4; Fe: 16.7 and 1.2; Co: 13.1 and 1.6. These values are within the reported ones for Mn(2+), Fe(2+) and Co(2+) in octahedral complexes [32–34], although below 25 K certain contribution from spin–orbit coupling could be present.

3.4. Magnetic properties

In the series, $T(Tzle)_2[Ni(CN)_4]$, the Ni atom in the $[Ni(CN)_4]$ unit preserves its square planar coordination to four CN ligands at the C end and remains in diamagnetic state. At low temperature, between T metals within the layer, the magnetic interactions must be of antiferromagnetic nature. These metal centers are distant above 10 Å and that interaction must be weak, because the super-exchange is taken over the T–N≡C–Ni–C≡N–T chain. Between T metal centers from neighboring layers the occurrence of a ferromagnetic interaction is possible, through the π–π cloud overlapping of neighboring molecules ring. Such behavior is observed for imidazole as intercalated molecules and it depends on the ring–ring distance [12]. The magnetic properties of this series of hybrid materials can be described as the interaction between seven identical paramagnetic centers forming an octahedral cluster compressed along the *z*-axis. The interaction between the metals located in the equatorial plane is of antiferromagnetic nature while it is ferromagnetic along the *z*-axis.

For $Ni(Tzle)_2[Ni(CN)_4]$ a rapid increase in the value of μ_{eff} is observed followed of a definite decrease (Fig. 4). This could be interpreted as coexistence of a very weak ferromagnetic interaction and an antiferromagnetic coupling, which dominates at very low temperatures. The recording of the magnetization curve with applied field (hysteresis loop) at 2 K suggests the presence of a weak ferromagnetic interaction at low temperature (see Supplementary information). The magnetization shows a small but reliable hysteresis, in correspondence with the effect observed for the temperature dependence of μ_{eff}. For Mn, Fe and Co such effect is not detected, probably because it is quite weak and the dominant interaction is that of the antiferromagnetic nature. For these last three metals only the antiferromagnetic interaction within the layer is detected (see Supplementary information).

The magnetic behavior for the series of thiazole intercalated solids is consistent with the structural information derived from the refined crystal structures (Table 1). The shortest ring-ring distance is observed for Ni, and for this composition is most favorable the presence of a ferromagnetic interaction between metal atom from neighboring layers, through π–π cloud overlapping of neighboring molecules ring. Also for Ni the stronger thiazole-metal coordination bond is observed (the shortest $T–N_{Tzle}$ distance). This is equivalent to the highest overlapping between the electron clouds of the metal and the ligand. These two factors determine the super-exchange integral through the bimolecular thiazole pillar and the value for the temperature where the magnetic ordering is possible.

For imidazole, a molecule with certain analogy with thiazole but with a greater dipole moment, at low temperature the ferromagnetic interaction dominates over the antiferromagnetic one for Co and Ni (see Supplementary information) [12]. This is ascribed to a strong attractive dipolar and quadrupolar interactions between imidazole molecules, compared with thiazole, and from this fact, to a stronger π–π cloud overlapping of neighboring molecules ring. Imidazole has a dipole moment of 3.860 versus 1.657 D for thiazole.

4. Conclusions

Thiazole molecules were intercalated in the series of layered solids, $T[Ni(CN)_4]$ with T = Mn, Fe, Co, Ni. The intercalated molecules occupy the axial coordination positions for the metal T, which results with a distorted octahedral coordination. The Ni atom preserves its planar coordination to four C end of CN groups. In the interlayers region molecules coordinated to neighboring layers are found interacting between them through their dipolar and quadrupolar moments. That cooperative dipolar and quadrupolar interactions between neighboring molecules make possible the existence of a stable 3D structure for the formed series of thiazole-intercalated materials, where the layers remain separated by bimolecular pillars. In addition to the structural study, the distortion for the octahedral coordination environment for the metal T, is also detected as spin–orbit coupling, with a pronounced temperature dependence for Fe and Co. The pronounced decrease observed for the effective magnetic moment below 25 K, reveals the contribution of zero-field splitting (ZFS) to the magnetic properties of this series of hybrid materials. At low temperature dominates the antiferromagnetic interaction between T metal centers within the layer, and only for T = Ni, a weak ferromagnetic effect was observed at 2 K. It seems, the ring–ring π–π cloud overlapping is insufficient to support a dominant ferromagnetic ordering of T metals from neighboring layers. This study shed light on the intermolecular interactions of thiazole molecules intercalated in 2D solids and contributes to understand the nature and properties of this type of hybrid inorganic–organic materials.

Acknowledgments

J.R.-H. thanks to SECITI-CLAF by the support provided for a post-doctoral fellowship through the project 025/2014. This study was partially supported by the CONACyT (Mexico) Projects 2011-01-174247, 2011-01-166387, and FON.INST./75/2012. The authors thank Dr. C. Aguirre for the thiazole molecule dipole and quadrupole moments calculation.

Appendix A. Supplementary data

CCDC 1046145, 1046142, 1046146 and 1046144 contains the supplementary crystallographic data for $Mn(Tzle)_2[Ni(CN)_4]$, $Fe(Tzle)_2[Ni(CN)_4]$, $Co(Tzle)_2[Ni(CN)_4]$ and $Ni(Tzle)_2[Ni(CN)_4]$. These data can be obtained free of charge via http://www.ccdc.cam.ac.uk/conts/retrieving.html, or from the Cambridge

Crystallographic Data Centre, 12 Union Road, Cambridge CB2 1EZ, UK; fax: (+44) 1223-336-033; or e-mail: deposit@ccdc.cam.ac.uk.

Supplementary data associated with this article can be found, in the online version, at http://dx.doi.org/10.1016/j.poly.2015.04.016.

References

[1] Y. Hijikata, S. Horike, M. Sugimoto, M. Inukai, T. Fukushima, S. Kitagawa, Inorg. Chem. 52 (2013) 3634.
[2] T.R. Cook, Y.-R. Zheng, P.J. Stang, Chem. Rev. 113 (2013) 734.
[3] D. Saha, Z. Bao, F. Jia, S. Deng, Environ. Sci. Technol. 14 (2010) 1820.
[4] M. Fischer, J.R.B. Gomes, M. Fröba, M. Jorge, Langmuir 28 (2012) 8537.
[5] A. Corma, H. García, F.X. Llabrés i Xamena, Chem. Rev. 110 (2010) 4606.
[6] P. Horcajada, C. Serre, G. Maurin, N.A. Ramsahye, F. Balas, M. Vallet-Regí, M. Sebban, F. Taulelle, G. Férey, J. Am. Chem. Soc. 130 (2008) 6774.
[7] L.E. Kreno, K. Leong, O.K. Farha, M. Allendorf, R. Van Duyne, J.T. Hupp, Chem. Rev. 112 (2011) 1105.
[8] J. Lee, O.K. Farha, J. Roberts, K.A. Scheidt, S.T. Nguyen, J.T. Hupp, Chem. Soc. Rev. 38 (2009) 1450.
[9] N.J. Hinks, A.C. McKinlay, B. Xiao, P.S. Wheatley, R.E. Morris, Microporous Mesoporous Mater. 129 (2010) 330.
[10] X.-Y. Wang, Z.-M. Wang, S. Gao, Chem. Commun. (2007) 1127.
[11] Z.-H. Xuan, D.-S. Zhang, Z. Chang, T.-L. Hu, X.-H. Bu, Inorg. Chem. 53 (2014) 8985.
[12] M. González, A.A. Lemus-Santana, J. Rodríguez-Hernández, M. Knobel, E. Reguera, J. Solid State Chem. 197 (2013) 317.
[13] F. Geng, R. Ma, Y. Ebina, Y. Yamauchi, N. Miyamoto, T. Sasaki, J. Am. Chem. Soc. 136 (2014) 5491.
[14] J.A. Rodríguez-Velamazán, M.A. González, J.A. Real, M. Castro, M.C. Muñoz, A.B. Gaspar, R. Ohtani, M. Ohba, K. Yoneda, Y. Hijikata, N. Yanai, M. Mizuno, H. Ando, S. Kitagawa, J. Am. Chem. Soc. 134 (2012) 5083.
[15] J. Rodríguez-Hernández, A.A. Lemus-Santana, J. Ortiz-López, S. Jiménez-Sandoval, E. Reguera, J. Solid State Chem. 183 (2010) 105.
[16] Y.M. Klein, N.F. Sciortino, F. Ragon, C.E. Housecroft, C.J. Kepert, S.M. Neville, Chem. Commun. (2014) 3838.
[17] A. Galet, A.B. Gaspar, M.C. Muñoz, G.V. Bukin, G. Levchenko, J.A. Real, Adv. Mater. 17 (2005) 2949.
[18] S. Bonhommeau, G. Molnár, A. Galet, A. Zwick, J.A. Real, J.J. McGarvey, A. Bousseksou, Angew. Chem., Int. Ed. 44 (2005) 4069.
[19] J. Rodríguez-Hernández, A.A. Lemus-Santana, C.N. Vargas, E. Reguera, C.R. Chim. 15 (2012) 350.
[20] J.T. Culp, C. Madden, K. Kauffman, F. Shi, C. Matranga, Inorg. Chem. 52 (2013) 4205.
[21] (a) Y. Li, Y. Liu, Y. Wang, Y. Leng, L. Xie, X. Li, Int. J. Hydrogen Energy 32 (2007) 3411;
(b) J.T. Culp, S. Natesakhawat, M.R. Smith, E. Bittner, C. Matranga, B. Bockrath, J. Phys. Chem. C 112 (2008) 7079.
[22] M. González, A.A. Lemus-Santana, J. Rodríguez-Hernández, C.I. Aguirre-Velez, M. Knobel, E. Reguera, J. Solid State Chem. 204 (2013) 128.
[23] G.M. Sheldrick, Program for Crystal Structure Determination, Institute fur Anorg, Chemie, Göttingen, Germany, 1997.
[24] A.L. Le Bail, ESPOIR: A Program for Solving Structures by Monte Carlo from Powder Diffraction Data, in EPDIC-7, Barcelona, 2000, http://www.cristal.org/sdpd/espoir/SS.
[25] J. Rodríguez-Carvajal, FULLPROF 2005 Program, Institute Louis Brillouin, Saclay, France, 2005.
[26] M.P. Shores, J.J. Sokol, J.R. Long, J. Am. Chem. Soc. 124 (2002) 2279.
[27] A.A. Lemus-Santana, M. González, J. Rodríguez-Hernández, M. Knobel, E. Reguera, J. Phys. Chem. A 117 (2013) 2400.
[28] E.G. Hohenstein, C.D. Sherrill, J. Phys. Chem. A 113 (2009) 878.
[29] Y. Zhang, Inorg. Chem. 21 (1992) 3889.
[30] R.L. Carlin, Magnetochemistry, Spinger-Verlag, Berlin, Heidelberg, New York, Toronto, 1986.
[31] R.S. Drago, Physical Methods for Chemists, Saunders College Publishing, Gainesville, 1962. 2nd ed.
[32] B.V. Behere, S. Mitra, Inorg. Chem. 19 (1980) 992.
[33] B.R. Garvey, J. Telser, Inorg. Chem. 51 (2012) 6000.
[34] Y.-Z. Zhang, W. Wernsdorfer, P. Pan, Z.-M. Wang, S. Gao, Chem. Commun. (2006) 3302.